Chinese Chemical Letters 34 (2023) 107326

Contents lists available at ScienceDirect

Chinese Chemical Letters

journal homepage: www.elsevier.com/locate/cclet

Nitrogen-doped pyrogenic carbonaceous matter facilitates azo dye decolorization by sulfide: The important role of graphitic nitrogen

Han-Qing Zhao[a,b], Wen-Qiang Li[a], Nannan Hou[a,*], Lei Li[a], Yiran Wang[a], Peili Lu[b], Yang Mu[a,*]

[a] CAS Key Laboratory of Urban Pollutant Conversion, Department of Environmental Science and Engineering, University of Science and Technology of China, Hefei 230026, China
[b] College of Environment and Ecology, Chongqing University, Chongqing 400044, China

ARTICLE INFO

Article history:
Received 22 December 2021
Revised 25 January 2022
Accepted 11 March 2022
Available online 14 March 2022

Keywords:
Azo dye
Decolorization
Graphitic N
Nitrogen doped graphene
Sulfide

ABSTRACT

Pyrogenic carbonaceous matter (PCM) catalyzes azo dye decolorization by sulfide, but the nitrogen doping catalytic mechanisms are poorly understood. In this study, we found that stagnate time of azo dye methyl orange (MO) decolorization was reduced to 0.54-18.28 min in the presence of various nitrogen-doped graphenes (NGs), remarkably lower compared to graphene itself. Particularly, graphitic nitrogen played a critical role in NGs-catalyzed MO decolorization by sulfide. Gas chromatography-mass spectrometry and *in-situ* surface Raman analysis demonstrated that doping nitrogen, especially graphite one facilitated reactive intermediate polysulfides formation. This is attributed to the improved electron conductivity through graphitic nitrogen doping, and the enhanced interactions between sulfide and carbon atoms bonded to graphitic nitrogen. This study not only provides a better understanding of PCM impact on transformations and fates of organic pollutants in natural environments, but also offer a new regulation strategy for more efficient wastewater treatment processes in PCM-catalyzed engineering systems.

Pyrogenic carbonaceous matter (PCM), including environmental black carbon (biomass char and fossil fuel soot), engineered carbons (activated carbon), and carbon nanomaterials (graphene and carbon nanotubes), constitute between 10% and 30% of organic carbon in sediments [1–4]. Traditionally, PCM has been merely viewed as a passive adsorbent for concentrating, capturing, and sequestering contaminants in an aquatic environment. Recent studies indicate that PCM could catalyze the reduction of various organic pollutants by sulfide coming from the microbial reduction of sulfate [2,5–8]. For example, black carbon facilitates trifluralin and pendimethalin abiotic reduction by sulfide, and graphene accelerates nitrobenzene degradation by sulfide [9,10].

The enhanced mechanisms of PCM for the reductive removal of various organic pollutants by sulfide are diverse. Some studies attributed the facilitation of carbon materials for pollutant reduction to oxygen functional groups, especially quinones on the surface of PCM that may help activate pollutant molecules and enhance electron transfer [9,11]. Other works demonstrate that the excellent electrical conductivity of carbon materials may play important roles in organic pollutants reduction by sulfide, enhancing electron transfer from sulfide to the pollutants and facilitating the formation of some critical intermediate [12,13]. Interestingly, our recent study discovered a new mechanism: PCM could reduce the stagnate phase of azo dye decolorization by sulfide, due to the formation of reactive intermediate polysulfides that react quickly with the azo dye [14]. This new finding further improves our understanding of PCM influence on the organic pollutants transformation under anaerobic aqueous conditions and particularly reveals the important role of polysulfides in transforming pollutants in natural environments. Occasionally, we observed that nitrogen-doped PCM could further reduce the stagnate phase of the azo dye decolorization by sulfide compared to that without nitrogen doping, while the reasons behind this phenomenon are unexplored.

The dopant of nitrogen in carbon materials, aimed at tuning their electronic features and hence the adsorption and catalytic properties, has been extensively studied in pollutant degradation [15,16]. For example, nitrogen-doped graphene effectively catalyzes the transformation of 4-nitrophenol to 4-aminophenol by $NaBH_4$, and carbon atoms next to the doped nitrogen atoms on graphene could serve as the active sites for the adsorption and activation of 4-nitrophenol [17]. Moreover, it was observed that nitrogen-doped carbon materials catalyze trichloroethylene degradation by sulfide [18]. On the other hand, different kinds of N species were dis-

* Corresponding authors.
E-mail addresses: hounan@ustc.edu.cn (N. Hou), yangmu@ustc.edu.cn (Y. Mu).

https://doi.org/10.1016/j.cclet.2022.03.049
1001-8417/

tributed on the surface of the nitrogen-doped materials, including pyridine N, pyrrole N, graphitic N, and N-oxide [17,19]. It has been demonstrated that these N species might play different roles in pollutant degradation [20,21]. Graphitic N on the surface of the nitrogen-doped materials plays a key role in impelling the reduction of nitroaromatics by $NaBH_4$ [22]. Nevertheless, Ding *et al.* indicated that pyridine N on the surface of the carbon materials appeared to play a critical role in trichloroethylene dichlorination by sulfide [18]. Up to now, the roles of nitrogen doping and different nitrogen species on PCM in catalyzing azo dye decolorization by sulfide remain unknown and deserve a careful investigation.

Therefore, the present study aimed to clarify the roles and the possible mechanisms of nitrogen doping and different nitrogen species on PCM mediated azo dye decolorization by sulfide. Methyl orange (MO), an azo dye widely used in chemical and textile industries, was chosen as the model pollutant [23–25]. Nitrogen-doped graphene (NG) was selected as a typical PCM. Firstly, we prepared various NGs with different N species contents by tuning the annealing temperature [18,26]. Then the catalytic performance of those NGs for MO decolorization by sulfide was studied. Afterward, the relationship between the catalytic performance of NGs and the N species relative contents was evaluated, emphasizing the influence of N doping on polysulfides formation, a key reactive intermediate. Moreover, the electrical conductivity test, polysulfides adsorption, and density functional theory (DFT) calculation were explored to further reveal the important roles of N in graphene on azo dye decolorization by sulfide.

MO, ammonia, urea, melamine, $(NH_4)_2S_n$, and elemental sulfur (S_0) were obtained from Sinopharm Chemical Reagent Co., Ltd. (China). Na_2S was purchased from Aladdin Industrial Corporation (China). All chemicals were used as received without further purification.

Reduced graphene oxide (RGO, 1–3 nmnm thickness, larger than 50 μm diameter, higher than 98% purity, and less than three layers) and graphene oxide (GO, 1–3 nm thickness, larger than 50 μm diameter, higher than 98% purity, and less than three layers) was obtained from Chengdu Organic Chemicals Company (China). NG was prepared using 50 mg RGO as the raw material and annealed at a predetermined temperature in an electric furnace [26,27]. For the NG with NH_3 as nitrogen precursor (NG_{amm}), 50 mg RGO was annealed under an atmosphere of 5% NH_3 and 95% Ar_2 at a rate of 100 mL/min, since a previous study demonstrated that nitrogen atom could be introduced to the graphene lattice with high temperature treatment under NH_3 atmosphere [28]. Afterward, during the annealing treatment for the graphene, the annealing temperature was increased at a rate of approximately 10 °C/min and held at T (T = 300, 400, 500, 600, 700, 800, 900, and 1000 °C) for 1 h, respectively, and then decreased at a rate of 10 °C/min until a temperature of 100 °C was reached. After that, the samples were further cooled to room temperature, washed by water, and then dried to remove impurities before use. The above-prepared graphene samples were coded as $NG_{amm\text{-}T}$. Additionally, the NG with GO precursor (named $NG_{GO\text{-}amm\text{-}T}$) was also prepared, in which the preparation method was similar with that of NG_{amm} except for GO precursor.

The morphological characterizations of the graphene materials and C, O, and N elemental mappings for the graphene samples were conducted on a scanning transmission electron microscope (STEM, JEM-ARM 2100F, JEOL, Japan). The surface atomic percent of C, O and N elemental composition and specific surface functional groups of the graphene materials were assessed using an XPS (ESCALAB 250, Thermo-VG Scientific Inc., USA). XPS patterns were measured in a 1.4×10^{-7} Pa vacuum at room temperature (22 °C). Curve fitting was performed using a Gaussian-Lorentzian peak shape after subtracting a Shirley background. A Raman spectrometer analyzed the defective level of graphene samples with an argon-ion laser excitation source at a 532 nm wavelength (LabRam HR, Horiba, France).

A physical property measurement system (PPMS, Dyna Cool, Quantum Design Inc., USA) measured the electrical conductivities of RGO and NG according to previous studies [29,30]. Specifically, the graphene samples were tablet compressed prior to measurement. Afterward, a four-electrode apparatus was fabricated using silver wires at two sides of the graphene tablet, two of the electrodes were used to input linearly changing direct current, and the other two electrodes were used to detect the output voltage. The following equation calculated the electrical conductivity of the graphene samples (σ) (Eq. 1):

$$\sigma = \frac{L}{RWD} \tag{1}$$

where L is the distance between the two electrodes outputting the voltage; R is the resistance; and W and D are the width and thickness of the graphene tablet, respectively.

MO decolorization experiments were conducted in 180 mL serum bottles containing 100 mL phosphate buffer solution (25 mol/L at pH 7.0) and 0.3 mmol/L MO in which 5 mg/L graphene material was mixed and then ultrasonic dispersed for 30 min. The solution was purged with nitrogen for at least 30 min to remove dissolved oxygen before placing it into the anaerobic operation box. Afterward, 1 mmol/L Na_2S stored in the anaerobic operation box was added to the serum bottle. After mixing with Na_2S, the solution was adjusted to pH 7.5 using 2 mmol/L HCl or NaOH solution. The decolorization reaction was conducted using an orbital shaker at 200 rpm in an anaerobic glove box at 30 °C under dark conditions. Compared with MO anaerobic reduction experiments, the difference for MO aerobic transformation experiment was it conducted at air conditions. Each experiment was performed at least in duplicate.

The liquid samples were taken at appropriate time intervals during the MO decolorization process and immediately filtered through 0.22 μm membrane (Jinten Co., China). The concentration of MO and their reductive products including *N*,*N*-dimethyl-*p*-phenylenediamine (DPD) and 4-aminobenzenesulfonic acid (ABS) were measured by high-performance liquid chromatography (HPLC) equipped with a diode array detector and a 4.6 mm × 250 mm Eclipse Plus C18 column at 30 °C (Agilent 1260, Agilent Technologies, USA). The flow rate of the mobile phase was 0.8 mL/min and the detection wavelengths were 270 (for DPD) and 254 nm (for MO and ABS). The composition of the mobile phase (A: methanol and B: 0.1% acetic acid/0.1% ammonium acetate) was as follows: 0 min: 5% A and 95% B, 15 min: 20% A and 80% B, 30 min 100% A and 0% B, 38 min: 5% A and 95% B [14].

The sulfide concentration in the solution was determined using the methylene blue method [31]. Gas chromatography-mass spectrometry (GC-MS, Thermo, Trace DSQ II, USA) analyzed the concentration of polysulfides (including disulfide, trisulfide and tetrasulfide in the range of 1 μmol/L to 1000 μmol/L) in the solution according to our previous study [14,32]. Sulfur species, including polysulfide and elemental sulfur on the surface of graphene, were determined by Raman spectrometer with an argon-ion laser excitation source of 532 nm (LabRam HR, Horiba, France) [33,34]. Graphene samples with sulfur species were freeze-dried and stored in an anaerobic operating box before analysis. Additionally, to eliminate the influence of oxygen on the transformation of sulfur species, the graphene samples were placed in anaerobic quartz sample cell for Raman analysis.

To understand further the role of various N species on PCM-mediated azo dye decolorization by sulfide, DFT calculations were conducted. The adsorption models for NG with sulfide were initially established by the commercialized software package Materials Studio 6.0. Configuration optimization steps were then car-

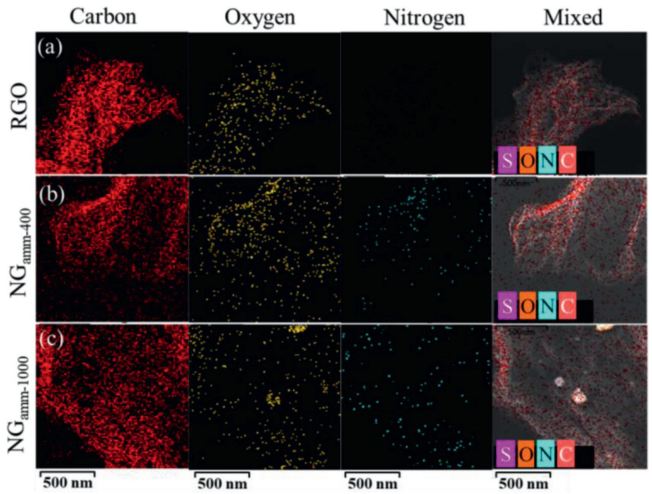

Fig. 1. STEM mapping images including C, O, N, and composite image for (a) RGO, (b) $NG_{amm\text{-}400}$, and (c) $NG_{amm\text{-}1000}$ samples, respectively.

Table 1
Relative N species contents in various NG_{amm}.

NG types	Pyridine N (%)	Pyrrole N (%)	Graphitic N (%)	N-oxide (%)
$NG_{amm\text{-}300}$	49.27	26.24	17.47	7.03
$NG_{amm\text{-}400}$	38.17	34.32	20.18	7.33
$NG_{amm\text{-}500}$	31.80	39.28	21.59	7.34
$NG_{amm\text{-}600}$	24.01	48.25	20.62	7.12
$NG_{amm\text{-}700}$	36.57	31.00	24.88	7.54
$NG_{amm\text{-}800}$	37.86	28.39	25.89	7.85
$NG_{amm\text{-}900}$	34.81	21.95	36.83	6.41
$NG_{amm\text{-}1000}$	22.19	25.70	39.21	12.90

ried out using the DMol3 module accompanied by the ultrasoft pseudopotentials to describe ion core and valence electrons [35,36]. Simultaneously, the generalized gradient approximation (GGA) method amended with Perdew and Wang (PW91) function combined with an all-electronic approach was used to explain the exchange-correlation functions [37]. Moreover, a conductor-like screening model (COSMO) simulated water media effects in actual processes [38]. During the geometric optimization process, the convergence threshold for the maximum energy change, force, and displacement were set to 2×10^{-5} Hartree, 4×10^{-3} Å, and 4×10^{-3} Å, respectively. The adsorption energy (ΔE_{ads}) was defined to indicate the adsorption capacity of the active species to the interface, the more negative the value of the adsorption energy, the stronger the corresponding adsorption capacity, and the following formula obtains it (Eq. 2):

$$\Delta E_{ads}(\text{species}) = E_{\text{species/substrate}} - E_{\text{species}} - E_{\text{substrate}} \quad (2)$$

where $E_{\text{species/substrate}}$, E_{species}, and $E_{\text{substrate}}$ represent the energy of the optimized adsorption model, adsorbate, and adsorbent, respectively.

Fig. 1 shows the STEM-EDS elemental mapping images of carbon, oxygen, and nitrogen for RGO and NG_{amm} samples. Compared to RGO (Fig. 1a), abundant nitrogen element was homogeneously distributed in NG_{amm} samples (Figs. 1b and c), indicating that nitrogen was successfully doped into the graphene. The total N content of NG_{amm} samples was in a range of 1.91% to 5.62%, and the elemental information of graphene samples from XPS is shown in Fig. S1 (Supporting information). Moreover, the N 1s spectrum of NG_{amm} samples can be fitted into four peaks (Fig. S2 in Supporting information), corresponding to pyridine N (398.3 eV), pyrrole N (399.6 eV), graphitic N (401.2 eV), and N-oxide (402.5 eV) [39]. Table 1 shows the relative N species contents in NG_{amm} samples calculated from XPS sub-peak results. In the $NG_{amm,}$ with the increase in annealing temperature, then graphitic N content increased, but pyridine N decreased, while the content of pyrrole N initially increased and then reduced.

Table 2
Estimated MO decolorization by sulfide kinetic values with different graphenes at 1 mmol/L Na_2S, 0.3 mmol/L MO, 5 mg/L catalyst, 30 °C, and pH 7.5.

Types	t_0 (min)	R^2 (%)
RGO	23.17 ± 2.16	98.8
$NG_{amm\text{-}300}$	8.25 ± 0.52	99.9
$NG_{amm\text{-}400}$	18.28 ± 1.21	99.6
$NG_{amm\text{-}500}$	7.15 ± 0.68	99.8
$NG_{amm\text{-}600}$	14.59 ± 0.92	99.7
$NG_{amm\text{-}700}$	3.96 ± 0.17	99.9
$NG_{amm\text{-}800}$	7.07 ± 0.28	99.9
$NG_{amm\text{-}900}$	1.27 ± 0.36	99.9
$NG_{amm\text{-}1000}$	0.54 ± 0.56	99.0

The MO decolorization process by sulfide in the presence of different kinds of graphene displayed in Fig. S3a (Supporting information) shows that all the NGs performed better than the RGO control. Similar to our previous study, the MO decolorization by sulfide with different NGs initially underwent a stagnate phase followed by a fast degradation phase. The Gompertz fitting model was used to simulate the MO decolorization process, and the detailed calculation method is shown in Supporting information [14]. As shown in Table 2 and Fig. S3b (Supporting information), the stagnate phase time (t_0) for the NG_{amm} mediated reaction ranged between 0.54 min and 18.28 min, remarkably lower than that of RGO (23.17 ± 2.16 min), suggesting nitrogen doping on PCM plays an essential role for azo dye decolorization by sulfide. Additionally, the reduction products of MO including DPD and ABS were also monitored. As shown in Fig. S4 (Supporting information), the final concentrations of DPD and ABS reached up to around 85% of the amount of MO degradation (0.3 mmol/L), and less than 15% unbalance of products might be due to the adsorption of graphene and instability of products DPD and ABS, which could further transform to other substances. These results indicated that both DPD and ABS were main products of MO reduction by sulfide. And the catalytic reactivity of $NG_{GO\text{-}amm}$ with GO precursor were also investigated (Fig. S5 in Supporting information), which showed poorer catalytic reactivity to reduce the stagnate phase time for MO reduction compared with $NG_{GO\text{-}amm}$ with RGO precursor.

For the effect of oxygen functional groups on the catalytic performance of NG, the XPS results in Fig. S1 showed that nitrogen doping treatment decreased the oxygen functional group contents of graphene, and the oxygen functional group contents decreased with the improvement of annealing temperature, while high temperature nitrogen doping treatment improved the catalytic performance of graphene. Thus, oxygen functional groups of graphene may not play the positive role in facilitating reduction of organic pollutants by sulfide. We also conducted MO decolorization by sulfide experiments with graphene treated at different annealing temperatures under Ar_2 atmosphere without nitrogen doping (Fig. S6 in Supporting information). The stagnate phase for the AG-mediated MO decolorization was longer than that of NG_{amm} at the same annealing temperature (Table S1 in Supporting information). The improvement of annealing temperature did not shorten the stagnate phase of AG-mediated MO decolorization by sulfide. These results further highlight the importance of nitrogen doping in promoting graphene-mediated MO decolorization by sulfide.

To understand which nitrogen species may play a role in NG-mediated MO decolorization by sulfide, the correlation between reaction stagnate phase time and N species content, including total N, graphitic N, pyridine N and pyrrole N, were further explored. As shown in Fig. 2, an evident negative linear correlation between the logarithm of the stagnate phase and the relative content of

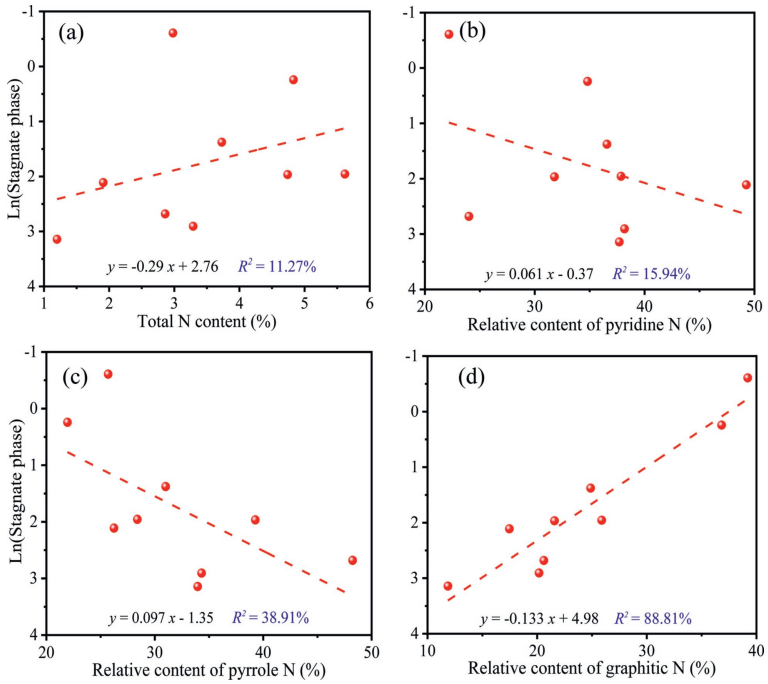

Fig. 2. Relationship between different nitrogen species content and catalytic efficiency of graphene toward MO degradation. (a) Total N, (b) pyridine N, (c) pyrrole N, (d) graphitic N. The catalytic efficiency is represented by the logarithm of the stagnate phase for different graphene-mediated MO decolorization.

graphitic N is obtained (R^2 = 88.82%). However, there is no apparent linear correlation between the logarithm of the stagnate phase and contents of total nitrogen, pyridine N, and pyrrole N species, as the R^2 values were below 50%. This result implies that graphitic N would likely be most important in NG-mediated MO decolorization by sulfide. Differently, Ding *et al.* indicated that pyridine N might play an important role in the trichloroethylene dechlorination by sulfide (R^2 = 97%) [18]. One of reasons to cause this difference may be owing to the different organic pollutants, in which the dechlorination of trichloroethylene in Ding's study while azo dye decolorization in our work. However, the impact of graphitic N on the dechlorination of trichloroethylene could not be excluded in the study from Ding *et al.*, with the correlation coefficient R^2 as high as 89% [18]. To further verify the role of graphitic N, we also prepared two NG samples with urea (NG_{urea}) or melamine (NG_{mela}) as nitrogen precursors under 800 and 1000 °C (the preparation procedure shown in Supporting information), respectively, and explored their catalytic performance on MO decolorization by sulfide. NG with higher relative content of graphitic N showed better catalytic performance, further demonstrating the important role of graphitic N in NG-mediating azo dye decolorization by sulfide (Fig. S7 in Supporting information).

Polysulfides are key reactive intermediates of azo dye decolorization by sulfide, and it was formed by the oxidation of sulfide and can react quickly with azo dye with the formation of elemental sulfur [14]. To prove that graphene facilitates the formation of polysulfide, the reaction that separates the processes of adding sulfide and MO (MO adding after 10 min pre-reaction between sulfide and graphene) was conducted. The results in Fig. S8 (Supporting information) showed that the stagnate phase time of MO reduction significantly decreased when sulfide pre-reacted with graphene for 10 min. This may be due to that graphene facilitated the transformation from sulfide to polysulfide, which can react quickly with MO. Additionally, the formation of polysulfides in the presence of different NGs was carefully explored in this work. GC-MS was used to detect the distribution of polysulfides concentration in aqueous solutions initially. As shown in Fig. 3a, for the RGO-mediated reaction, polysulfides concentration reached a maximum value of 600 μmol/L in the first 40 min of reaction, then reduced until the reaction finished. A similar trend was found in the NG_{amm}-mediated MO decolorization process; however, it took less time (10–30 min) for the polysulfides concentration to reach a maximum value. Nevertheless, the maximum concentration of polysulfides in NG added systems was 200-550 μmol/L, lower than that of RGO with about 550 μmol/L, which may be due to the stronger adsorption capacity of NG to polysulfides compared with RGO, which will be discussed below.

Raman spectra were used to study the distribution of sulfur species on the surface of different graphenes. Fig. 3b shows the Raman spectra of RGO and $NG_{amm\text{-}1000}$ at 10 and 40 min of the MO decolorization process. Four Raman peaks at 50, 146, 210 and 460 cm^{-1} appeared for the $NG_{amm\text{-}1000}$ samples after 10 min of MO decolorization reaction, while there was no significant Raman peak in the RGO sample. After 40 min of reaction, the intensity of the four Raman peaks in $NG_{amm\text{-}1000}$ samples further increased, while four similar Raman peaks started to appear on the surface of RGO samples. According to the Raman spectra of standard sulfur species in Fig. S9 (Supporting information), the Raman peaks that appeared during the MO decolorization process may be attributed to elemental sulfur (49, 152, 216 and 470 cm^{-1}) and polysulfides (51 and 450 cm^{-1}). Related studies indicate that elemental sulfur combines quickly with sulfide with the formation of polysulfide [40,41]. Therefore, above results suggest that graphene modification by nitrogen doping facilitates the polysulfides formation during MO decolorization by sulfide.

The polysulfides adsorption abilities of different kinds of graphene were also investigated, and the details of adsorption experiments are provided in Supporting information. The UV-vis absorption spectra variations of the polysulfide solution after graphene adsorption suggest that the polysulfides adsorption ability of N doping was higher than that of RGO (Fig. S10 in Supporting information). A previous study showed that nitrogen doping treatment facilitated the adsorption of polysulfides to a graphene sponge [42]. This may explain why the maximum polysulfides con-

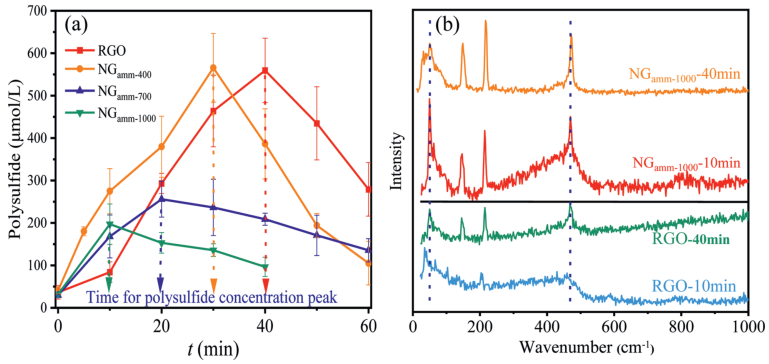

Fig. 3. (a) Polysulfides formation (C = disulfide × 2 + trisulfide × 3) for the RGO, NG$_{amm-400}$, NG$_{amm-700}$ and NG$_{amm-1000}$ during the MO decolorization process. (b) Raman spectra of graphene samples that participated in the MO decolorization process for 10 and 40 min, respectively.

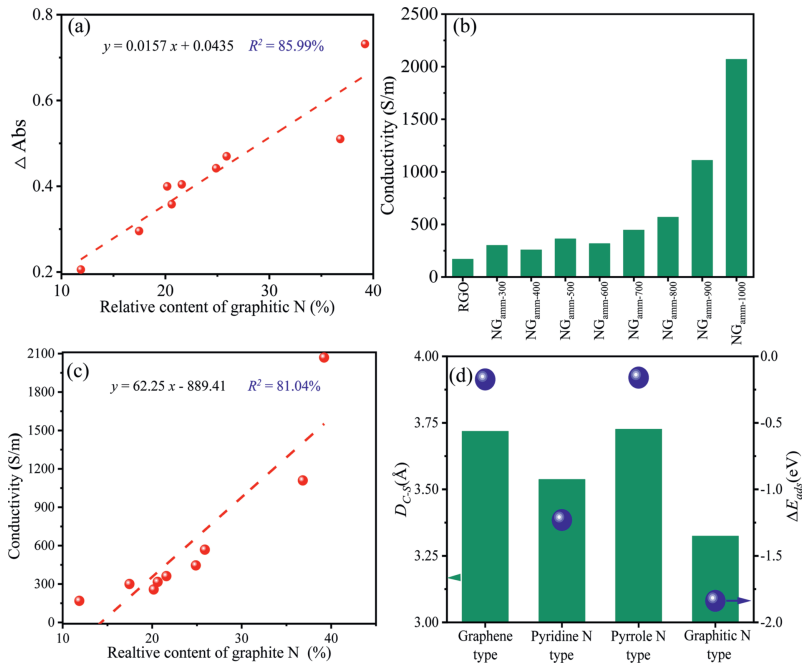

Fig. 4. (a) Relationship between relative content of graphitic N and variation value (before and after it adsorbed by graphene) for polysulfides UV-vis absorption peak intensity at 230 nm; (b) electrical conductivity of various graphenes; (c) relationship between electrical conductivity and relative content of graphitic N for graphene; and (d) the bond length and adsorption energy of sulfide adsorbed on four kinds of graphene configurations.

centration in NG-mediated systems was lower during the MO decolorization process than in RGO-mediated ones. Interestingly, a good positive linear correlation between the relative content of graphitic N and adsorbed polysulfides amount was obtained, as shown in Fig. 4a. The absorbance difference at 230 nm before and after absorption by graphene was used to represent the adsorbed polysulfide amount. This result indicates that graphitic N species enhance the polysulfides adsorption ability of NG, resulting in the faster achievement of critical reaction concentration of polysulfides [14], thus reducing the stagnate phase length of azo dye decolorization by sulfide.

On one hand, the electrical conductivity of different kinds of graphenes was analyzed. As shown in Fig. 4b, nitrogen doping improved the electrical conductivity of graphene, consistent with previous studies [43,44]. In particular, there was a good positive correlation between electrical conductivity and the relative graphitic N content of NG$_{amm}$, while no significant correlation with content of total N, pyridine N and pyrrole N (Fig. 4c and Figs. S11a–c in Supporting information). It has been demonstrated that graphitic N can preserve its high carrier mobility due to minor distortion of the graphene lattice [43,45]. Moreover, graphitic N infuses excess electrons in a carbon matrix, enhancing electrical conductivity for carbon materials [12,46]. Consequently, the improved electrical conductivity of NGs, majorly resulting from the presence of graphitic N, may benefit electron transfer from sulfide species to MO, thus facilitating the polysulfides formation that can react with MO quickly.

On the other hand, the NG$_{amm-800}$ and NG$_{amm-1000}$ nanosheets showed a crinkled and partially aggregated structure compared with the silk veil-like morphology of RGO (Fig. S12 in Supporting information). This is possibly due to the formation of a defective structure and refabrication of graphene layers during the nitrogen doping process which is in accordance with a previous report [15]. The D and G peaks intensity ratio (I_D/I_G) from Raman spectroscopy was used to reflect the defective level of graphene samples (Fig. S13a in Supporting information). The NG$_{amm}$ samples I_D/I_G value in the range of 0.97 to 1.25 was higher than that of RGO samples (Fig. S13b in Supporting information), suggesting that more defects could be introduced to the carbon matrix of graphene with nitrogen doping, especially under high graphitic N conditions. Correlation analysis showed a good positive linear correlation between defective level and conductivity of NG (Fig. S11d

in Supporting information). Thus, the improvement of conductivity for NG may be majorly owing to the defective from graphitic N species. We adopted DFT calculations to explore further the impact of carbon matrix defects from nitrogen doping on polysulfides formation. First, four graphene configurations, including carbon matrix of graphene, pyridine N, pyrrole N, and graphitic N, together with the adsorbed sulfide, were optimized (Fig. S14 in Supporting information). As shown in Table S2 (Supporting information) and Fig. 4d, the adsorption energy of sulfide on the graphene carbon matrix was −0.17 eV, higher than the N-containing configurations adsorption energies of −1.23, −0.16 and −1.84 eV for pyridine N, pyrrole N, and graphitic N, respectively. Moreover, the C–S bond lengths for pyridine N, pyrrole N and graphitic N configurations were 3.537, 3.726 and 3.324 Å, respectively, lower than that between sulfide and carbon matrix of graphene (3.718 Å), as shown in Fig. 4d. In particular, the graphitic N configuration showed the lowest adsorption energy and the shortest C-S bond length. The above results may be due to the strong electron attracting ability of nitrogen atoms, especially that of graphitic N compared with carbon atoms, the carbon atoms adjacent to nitrogen possess partial positive charges, advantageous for the interaction between anionic sulfide and positively charged carbon atoms bonded to nitrogen atoms [47,48]. After sulfide bonding with NG, the excellent electrical conductivity of NG rooting from graphitic N improved the electron transfer from sulfide to organics with the formation elemental sulfur, and the formed elemental sulfur can combine quickly with sulfide with formation of polysulfide, and it consequently speeding up the decolorization of azo dye.

This work demonstrated that nitrogen doping into PCM could promote the formation of reactive intermediate polysulfides, thus reducing the stagnate phase of azo dye decolorization by sulfide. We found for the first time that graphitic N of PCM would play a significant role in this decolorization process, majorly due to improvement of the PCM electrical conductivity for electron transfer and enhancement of the bonding ability between carbon matrix and sulfide. Our study not only provides a better understanding of the impacts of broadly-presented PCM on the transformations and fates of sulfur species and organic pollutants in sediments, ground water and even municipal wastewater (Fig. S15 in Supporting information showed graphene also promoted MO decolorization by sulfide under aerobic conditions), but also offers a new strategy to achieve more efficient wastewater treatment processes in engineered systems by regulating the amount and type of nitrogen in PCM.

Declaration of competing interest

The authors declare that they have no known competing financial interest or personal relationships that could have appeared to influence the work reported in this paper.

Acknowledgment

The authors wish to thank theNational Natural Science Foundation of China (Nos. U19A20108, 52025101, 51821006 and 51878637) for financially supporting this study.

Supplementary materials

Supplementary material associated with this article can be found, in the online version, at doi:10.1016/j.cclet.2022.03.049.

References

[1] J.J. Middelburg, J. Nieuwenhuize, P. van Breugel, Mar. Chem. 65 (1999) 245–252.
[2] J.J. Pignatello, W.A. Mitch, W. Xu, Environ. Sci. Technol. 51 (2017) 8893–8908.
[3] H.Q. Zhao, Q. Liu, Y.X. Wang, et al., Chem. Eng. J. 351 (2018) 912–921.
[4] M. Zhu, L. Zhang, S. Liu, et al., Chin. Chem. Lett. 31 (2020) 1961–1965.
[5] Q. Liu, H.Q. Zhao, L. Li, et al., J. Hazard. Mater. 357 (2018) 235–243.
[6] W. Xu, J.J. Pignatello, W.A. Mitch, Environ. Sci. Technol. 49 (2015) 3419–3426.
[7] R.G. Luthy, G.R. Aiken, M.L. Brusseau, et al., Environ. Sci. Technol. 31 (1997) 3341–3347.
[8] E.J. Weber, R.L. Adams, Environ. Sci. Technol. 29 (1995) 1163–1170.
[9] H. Fu, D. Zhu, Environ. Sci. Technol. 47 (2013) 4204–4210.
[10] W. Gong, X. Liu, S. Xia, et al., J. Hazard. Mater. 310 (2016) 125–134.
[11] H.J. Amezquita-Garcia, E. Razo-Flores, F.J. Cervantes, et al., Carbon 55 (2013) 276–284.
[12] W. Xu, J.J. Pignatello, W.A. Mitch, Environ. Sci. Technol. 47 (2013) 7129–7136.
[13] S.Y. Oh, J.G. Son, O.T. Lim, et al., Environ. Geochem. Health 34 (2012) 105–113.
[14] H.Q. Zhao, S.Q. Huang, W.Q. Xu, et al., Environ. Sci. Technol. 53 (2019) 4397–4405.
[15] X. Duan, Z. Ao, H. Sun, et al., ACS Appl. Mater. Interfaces 7 (2015) 4169–4178.
[16] X.H. Jiang, L.S. Zhang, H.Y. Liu, et al., Angew. Chem. Int. Ed. 59 (2020) 23112–23116.
[17] X.K. Kong, Z.Y. Sun, M. Chen, et al., Energy Environ. Sci. 6 (2013) 3260–3266.
[18] L. Ding, P. Zhang, H. Luo, et al., Environ. Sci. Technol. 52 (2018) 14286–14293.
[19] L. Panchakarla, K. Subrahmanyam, S. Saha, et al., Adv. Mater. 21 (2009) 4726–4730.
[20] F. Yu, L. Wang, Q. Xing, et al., Chin. Chem. Lett. 31 (2020) 1648–1653.
[21] L.S. Zhang, X.H. Jiang, Z.A. Zhong, et al., Angew. Chem. Int. Ed. 60 (2021) 21751–21755.
[22] F. Yang, C. Chi, C. Wang, et al., Green Chem. 18 (2016) 4254–4262.
[23] V.K. Gupta, R. Kumar, A. Nayak, et al., Adv. Colloid Interface Sci. 193 (2013) 24–34.
[24] Y. Yao, H. Bing, X. Feifei, et al., Chem. Eng. J. 170 (2011) 82–89.
[25] E. Forgacs, T. Cserhati, G. Oros, Environ. Int. 30 (2004) 953–971.
[26] Y.X. Wang, W.Q. Li, C.S. He, et al., Biosens. Bioelectron. 160 (2020) 112231.
[27] E. Yoo, J. Nakamura, H. Zhou, Energy Environ. Sci. 5 (2012) 6928–6932.
[28] X. Chen, W.D. Oh, Z.T. Hu, Appl. Catal. B Environ. 225 (2018) 243–257.
[29] K.A. Borup, J. de Boor, H. Wang, et al., Energy Environ. Sci. 8 (2015) 423–435.
[30] M. Zhou, T. Tian, X. Li, et al., Int. J. Electrochem. Sci. 9 (2014) 810–820.
[31] R. Sun, L. Zhang, Z. Zhang, et al., Water Res. 131 (2018) 239–245.
[32] T. Zeng, K.L. Ziegelgruber, Y.P. Chin, et al., Environ. Sci. Technol. 45 (2011) 6814–6822.
[33] G. Janz, J. Downey, E. Roduner, et al., Inorg. Chem. 15 (1976) 1759–1763.
[34] J.T. Yeon, J.Y. Jang, J.G. Han, et al., J. Electrochem. Soc. 159 (2012) A1308.
[35] L. Zhou, S.W. Yang, M.F. Ng, et al., J. Am. Chem. Soc. 130 (2008) 4023–4027.
[36] B. Kang, H. Liu, J.Y. Lee, Phys. Chem. Chem. Phys. 16 (2014) 974–980.
[37] D. Vanderbilt, Phys. Rev. B 41 (1990) 7892.
[38] A. Klamt, V. Jonas, T. Bürger, et al., J. Phys. Chem. A 102 (1998) 5074–5085.
[39] Z. Du, X. Chen, W. Hu, et al., J. Am. Chem. Soc. 141 (2019) 3977–3985.
[40] R. Hedderich, O. Klimmek, A. Kröger, et al., FEMS Microbiol. Rev. 22 (1998) 353–381.
[41] A. Kletzin, T. Urich, F. Müller, J. Bioenerg. Biomembr. 36 (2004) 77–91.
[42] G. Zhou, E. Paek, G.S. Hwang, et al., Nat. Commun. 6 (2015) 7760.
[43] H.C. Youn, S.M. Bak, M.S. Kim, et al., ChemSusChem 8 (2015) 1875–1884.
[44] T. Van Khai, H.G. Na, D.S. Kwak, et al., J. Mater. Chem. 22 (2012) 17992–18003.
[45] C. Li, Y. Hu, M. Yu, et al., RSC Adv. 4 (2014) 51878–51883.
[46] X. Wang, G. Sun, P. Routh, et al., Chem. Soc. Rev. 43 (2014) 7067–7098.
[47] T. Ikeda, M. Boero, S.F. Huang, et al., J. Phys. Chem. C 112 (2008) 14706–14709.
[48] H. Watanabe, S. Asano, S.I. Fujita, et al., ACS Catal. 5 (2015) 2886–2894.